energies

MDPI

Article

Analysis of the Implementation of Effective Grounding in 400 kV Overhead Lines

Michał Borecki *, Paweł Kluge and Maciej Ciuba

Institute of Theory of Electrical Engineering, Warsaw University of Technology, 00-662 Warsaw, Poland
* Correspondence: michal.borecki1@pw.edu.pl

Abstract

Grounding is one of the key elements ensuring the reliable operation of overhead lines. The purpose of this paper is to provide a comprehensive assessment of grounding using a 400 kV overhead line as an example. The paper presents the results of diagnostic grounding measurements of various types of 400 kV overhead line poles, performed according to technical documentation and taking into account local terrain characteristics. The paper examines a large number of overhead line poles in both uniform and varied terrains, taking into account soil conditions based on geotechnical documentation. Furthermore, the paper presents a simulation analysis of lightning current dissipation through the grounding of a selected pole, taking into account geotechnical soil investigations with respect to soil stratification. The final section of the paper includes guidelines on grounding and assessment of the technical condition of grounding systems, which may be useful to transmission and distribution network operators.

Keywords: finite element method (FEM); transient field distribution; overhead line; power grids; grounding; measurements

Check for updates

Academic Editor: Salvatore Celozzi

Received: 23 September 2026
Revised: 28 October 2026
Accepted: 1 November 2026
Published: 6 November 2026

Copyright: © 2026 by the authors. Licensee MDPI, Basel, Switzerland. This article is an open access article distributed under the terms and conditions of the Creative Commons Attribution (CC BY) license.

1. Introduction

The rapid development of modern power grids and the increasing transmission capacity of overhead lines require an increasingly detailed approach to ensuring their reliable operation, particularly in the context of atmospheric overvoltages and transient phenomena in high-voltage networks [1,2]. Overhead lines, which provide connections between substations, are a key element of the power grid. Furthermore, due to the development of increasingly powerful renewable energy sources located in different areas and climate zones, grounding must be carefully considered.

Grounding is crucial for ensuring the reliable operation of overhead lines and substations under surge conditions [3,4]. The performance of grounding systems depends on several factors, including soil type, grounding configuration and the number of grounding electrodes, soil resistivity, and climatic conditions [5,6].

The literature presents detailed models of grounding systems subjected to atmospheric overvoltages, accounting for the interaction between grounding systems and soils of varying resistivities [7,8]. Other studies analyze the impact of lightning currents on touch and step voltages, highlighting the importance of soil properties and frequency-dependent soil behavior in the analysis of grounding systems [9,10].

Adequate grounding resistance for overhead lines is a crucial factor in ensuring their reliable operation. Previous research has examined grounding resistance under various conditions, including the grounding of transmission line towers and seasonal variations

in tower grounding impedance [5,6]. Numerous studies have also investigated lightning discharges and their impact on transmission line systems [3,4].

Another significant area of research concerns soil ionization phenomena that occur when high-magnitude current impulses flow through grounding systems [11,12].

The development of renewable energy sources, including large-scale wind and photovoltaic power plants, has also increased the importance of the proper design and analysis of grounding systems [13,14]. Numerical methods, including the finite element method (FEM), method of moments, and finite-difference time-domain (FDTD) method, are used to investigate grounding and electromagnetic phenomena in power systems [7,12].

A large number of simulation analysis results can be found in the literature [15,16]. These studies primarily concern the mutual coupling of grounding systems installed on overhead lines when subjected to surge currents [17,18]. Many simulation studies also analyze soil ionization phenomena resulting from the flow of surge current through the grounding system [19]. Collectively, the results of these studies indicate that the transient response of grounding systems depends on soil properties, the grounding system configuration, and the characteristics of the driving current [7,9–12,19–23].

Field studies on actual transmission line towers are also described in the literature, providing data on grounding resistance and impedance under real-world conditions [6,21]. Numerical studies are additionally employed to analyze the transient response of tower grounding systems and the spatial distribution of electric potential during a lightning current discharge [13,18].

These studies highlight the importance of both experimental measurements and numerical analyses; however, they generally focus on specific aspects of grounding system behavior—such as seasonal variations, frequency dependence, soil ionization, or individual grounding system configurations.

Low-resistivity materials—such as foundation concrete, bentonite, and cement—can be used in grounding systems installed in high-resistivity soils exceeding 1000 Ωm. The use of such materials, combined with the need to account for multilayered soil structures, requires knowledge of the actual geotechnical conditions at the tower sites under investigation.

Lightning current parameters, including peak value and rise time, also influence the response of transmission line grounding systems. Lightning strikes may consist of multiple component strokes; the current of the first stroke can have a peak value below 50 kA and a rise time of less than 7 μs [8,20].

This study analyzes actual 400 kV overhead line towers located in various areas. Field measurements were conducted on the tower grounding systems, covering sites with similar soil and climatic conditions as well as selected sites with differing geotechnical conditions. The sites under investigation are located in a European country with a temperate climate.

Unlike previous studies [7,12,21], this work combines the following aspects: the execution and analysis of field measurements of grounding resistance at low frequency at multiple tower sites of a 400 kV line, and a three-dimensional finite element method (FEM) analysis of lightning current distribution under transient conditions. This approach enables a comprehensive assessment of the properties of grounding systems under the conditions considered.

Field measurements were limited to determining the tower-footing grounding resistance under low-frequency test conditions. The numerical part was treated separately and addressed the transient response of the selected grounding system to a prescribed lightning-current excitation. The FEM analysis complements the field measurements by providing the spatial and temporal distributions of electric potential and current density. The measured grounding resistance is therefore not used as a direct representation or validation of the transient grounding impedance.

The soil conditions under study were characterized using multilayer soil models developed from geotechnical surveys conducted at the tower sites, accounting for soil layers down to a depth of 7 m and the groundwater level. Additional grounding configurations included 1.5 m and 3 m long grounding rods located at selected points near the tower.

The analysis of the 400 kV transmission-tower grounding system combined field measurements with finite-element simulations in ANSYS. For the transient numerical study, a 10/350 μs double-exponential current waveform with an approximately 100 kA peak value was adopted as a high-amplitude reference case.

Despite significant progress in the experimental and numerical study of grounding systems, comprehensive assessments of actual high-voltage transmission tower grounding systems remain relatively limited. There is a need for research that combines field measurements taken on actual transmission towers under various soil conditions with numerical analyses of transient electric potential and current density distributions within the grounding systems. This approach is crucial because the power-frequency grounding resistance obtained from field measurements characterizes the system's overall effectiveness under test conditions, while simulation analysis provides additional insights into the spatial response of the grounding system when subjected to lightning current. Integrating these approaches enables a more comprehensive interpretation of the behavior of grounding systems for actual high-voltage poles.

The primary contribution of this work is the combined assessment of actual grounding systems of 400 kV overhead-line towers using field measurements, site-specific geotechnical information, and three-dimensional transient FEM analysis. The experimental and numerical parts address different electrical conditions: the measurements characterize low-frequency grounding resistance, whereas the numerical model predicts transient spatial distributions of electric potential and current density under the adopted lightning-current excitation and soil-model assumptions.

The study comprises the following elements: (i) assessment of the grounding resistance of actual 400 kV overhead line towers based on field measurements under various soil conditions; (ii) comparative analysis of measured grounding effectiveness across different locations; (iii) application of a finite element model of the actual grounding system of a selected tower to determine the spatial distribution of electric potential and current density under a specified transient excitation; and (iv) analysis of experimental and numerical results as complementary approaches to evaluating the effectiveness of the grounding system.

The paper is organized as follows. Section 2 presents the results of field measurements of grounding resistance. Section 3 describes the finite element model developed in Ansys. Section 4 presents and discusses the obtained results and their application to diagnostics of grounding systems. Finally, Section 5 summarizes the main conclusions of the study.

2. Materials and Methodology

As part of a broader analysis of the effectiveness of grounding installations in high-voltage overhead lines, 16 pole positions located in geotechnically diverse areas were analyzed. An example of the grounding arrangement used for the poles of the transmission line under study is shown in Figure 1. The pole grounding system utilized a TU12-15/10 type arrangement. It consisted of a 25 × 4 mm steel grounding strip and Galmar grounding rods with a diameter of 17.2 mm and lengths of 1.5 m and 3 m. For the specific pole in question, two 3 m rods and four 1.5 m rods were used. For comparison purposes, eight poles located close together within a stay section and eight poles located in different sections in geotechnically diverse areas were considered. Therefore, this article presents a comparison of two groups, each comprising eight measurement sites. This enabled an analysis of the impact of differences in local geotechnical conditions and grounding system configurations.

The grounding resistance was measured using the three-electrode method with two auxiliary probes. The measurement setup comprised the grounding system under test and two auxiliary electrodes: a voltage electrode and a current electrode. Measurements were performed using a Sonel MRU-200 (SONEL S.A., Świdnica, Poland) earth resistance meter. The meter was connected to the grounding system under test and to both auxiliary electrodes via separate test leads. Measurements were performed in accordance with IEEE Std 81, IEEE Guide for Measuring Earth Resistivity, Ground Impedance, and Earth Surface Potentials of a Grounding System. The measurement configuration diagram is shown in Figure 2.

The geotechnical analysis of the areas included examining the soil category and its layers at a depth of up to 7 m and determining the water level within the considered poles. The individual pole locations were characterized by diverse soil profiles, comprising cohesive and non-cohesive soils as well as combinations of various geotechnical units. Groundwater levels also varied across the analyzed sites. These data served to characterize the actual site conditions under which the grounding resistance measurements were performed.

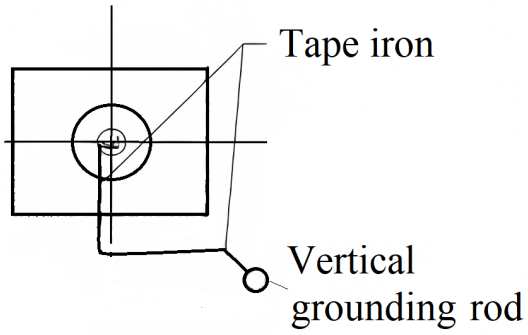


Figure 1. Schematic drawing of the grounding location at the foundation.

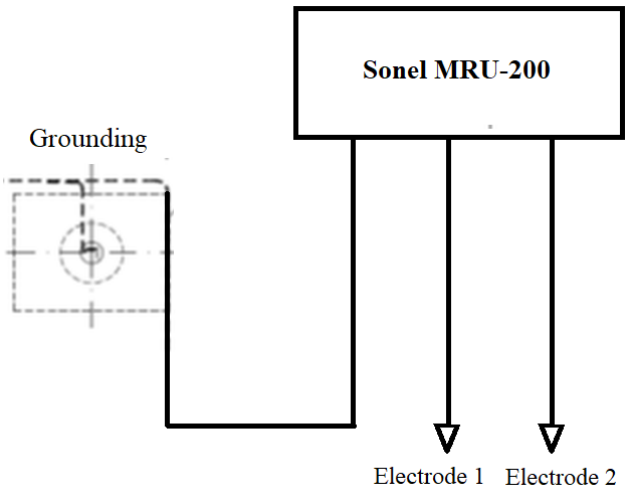


Figure 2. Schematic diagram of the three-electrode measurement of pole grounding resistance, where electrode 1 is the voltage electrode, electrode 2 is the current electrode, y is the distance between the grounding system under test and the current electrode, and x is the distance between the grounding system and the voltage electrode.

The experimental and numerical parts of the study were used to investigate different aspects of the grounding-system behavior. The three-electrode measurements were used to determine the low-frequency grounding resistance of the investigated tower grounding systems, whereas the transient FEM analysis was used to investigate the spatial and temporal distributions of electric potential and current density under a prescribed transient-current

excitation. Consequently, the grounding resistance obtained from the field measurements is not treated as being equivalent to the transient grounding impedance during lightning current excitation. The geotechnical data were subsequently used to define the geometrical stratification of the soil domain considered in the numerical model of the selected tower location.

The analysis is presented in two formats: measured values and values calculated taking into account ground conditions. Measured values were obtained directly from field measurements, whereas calculated values were determined using correction factors that account for local soil conditions.

The measured values show that the deviations in the obtained results, with the exception of one pole, are within the range of 2–2.5 Ω. At the same time, virtually all results meet the standard requirements for grounding resistance [24,25]. The measurements were performed for grounding systems installed in accordance with the technical documentation, taking into account local terrain conditions. In the case of converted values, the grounding resistance level for a uniform area (Figure 3) is higher compared to the resistance level obtained for different areas (Figure 4). The grounding systems under investigation were constructed using a specific grounding configuration and conductive elements, with the layout adapted to the local conditions at each pole location. Subsequently, the measurement procedure was applied to the installed grounding systems under actual field conditions.

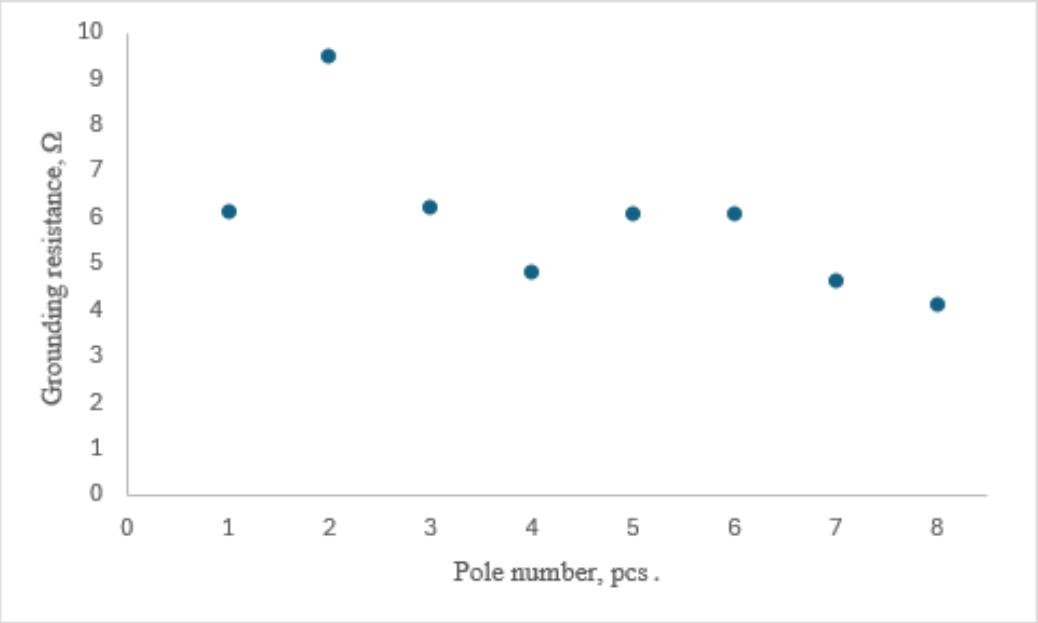


Figure 3. Measured grounding resistance for towers located within one relatively uniform area.

This is influenced by the soil in which the grounding is installed. However, in the authors' opinion, the greatest influence is the grounding design (the number and length of the rods used) and the quality of the connection/grounding method.

As can be seen, the individual grounding design for each site impacts the final results. For the relatively uniform area, the designed grounding systems included combinations of eight rods with lengths of 1.5 m and 3 m. The rods were arranged at two locations near the tower.

For the geotechnically diverse locations, the designed grounding systems included combinations of seven rods with lengths of 1.5 m and 3 m. The rods were arranged at a single location, with a total rod length of 18 m.

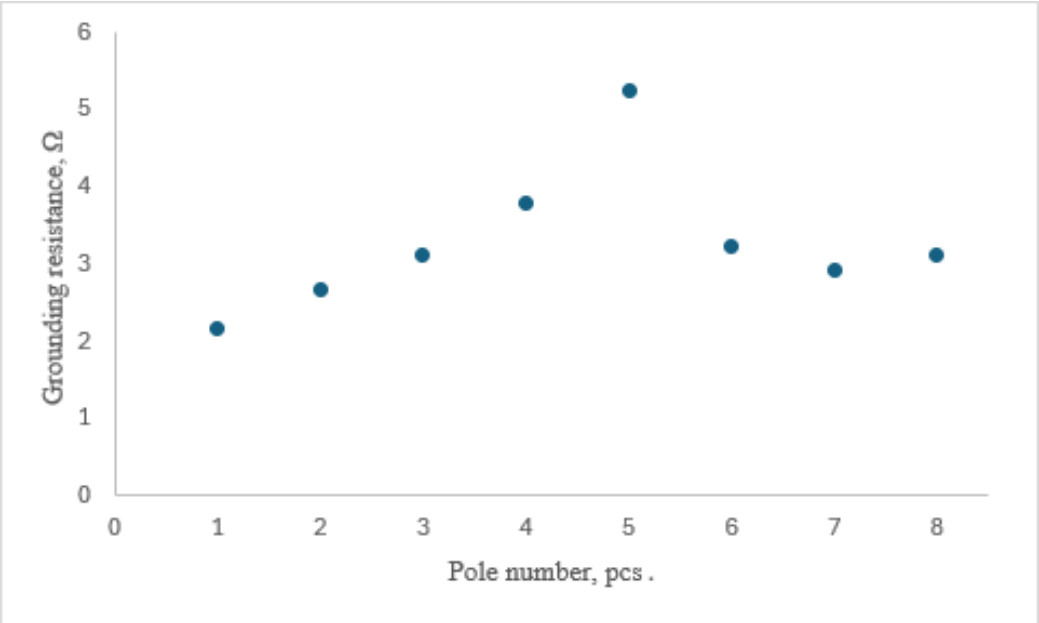


Figure 4. Measured grounding resistance for towers located in geotechnically diverse areas.

Therefore, it can be concluded that the grounding design influenced the obtained results, as the soil parameters were factored into the appropriate coefficients during the calculation (Figure 5). For one area, this coefficient was 1.2 [24]. For different areas, the coefficient ranged from 1.2 to 2 [24]. This is due to the difficult ground conditions. The measurements were performed when the ground was damp or very wet.

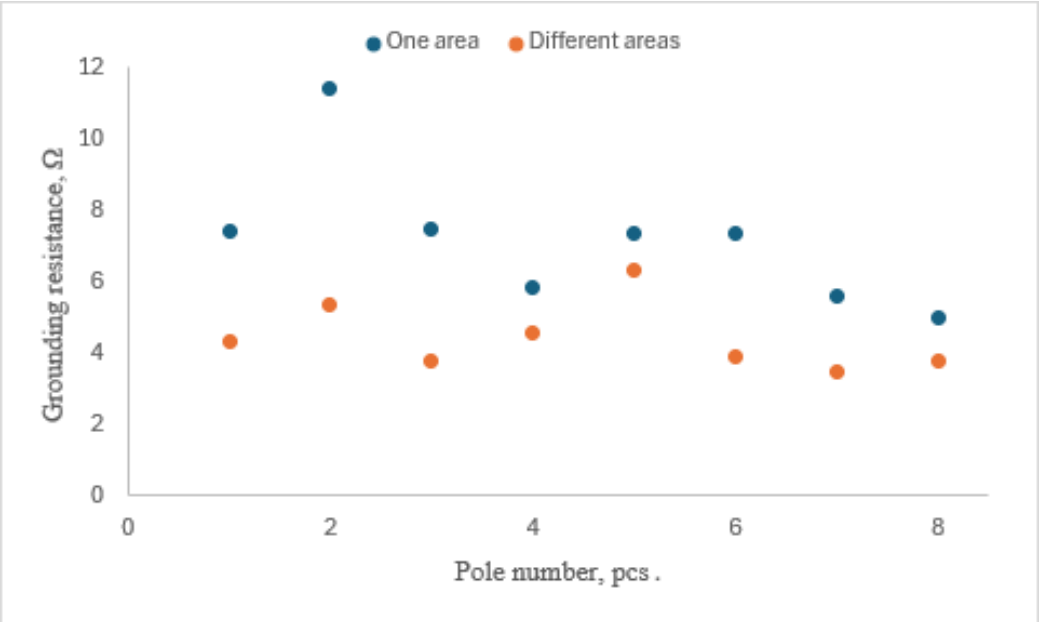


Figure 5. Grounding-resistance values corrected for local soil conditions for the relatively uniform and geotechnically diverse areas.

Based on the measurements and calculations, the Type A measurement uncertainty is approximately 0.33 for diverse areas and 0.58 for a single area. This is due to the difficult geotechnical conditions and the analyzed dataset.

Moreover, for a uniform area, the water level is at a height of 1 m. However, most pole positions in diverse areas are located where the water level is at a height of 0 m. Such

circumstances significantly complicate the installation and ensure the standard values of grounding resistance.

3. Results

3.1. Numerical Model of the Selected Tower Grounding System

As part of the simulation analysis, a model of the pole's grounding system was created, taking into account the soil layers based on geotechnical documentation (Figure 6).

The final three-dimensional numerical model was solved in ANSYS Electronics Desktop 2026 R1 using the Maxwell 3D Electric Transient solver. The model included the metallic tower structure, the grounding system, and the surrounding soil represented by individual layers according to the available geotechnical documentation. The transient analysis was performed in the time domain to determine the electric-potential and current-density distributions within the grounding system and the surrounding soil.

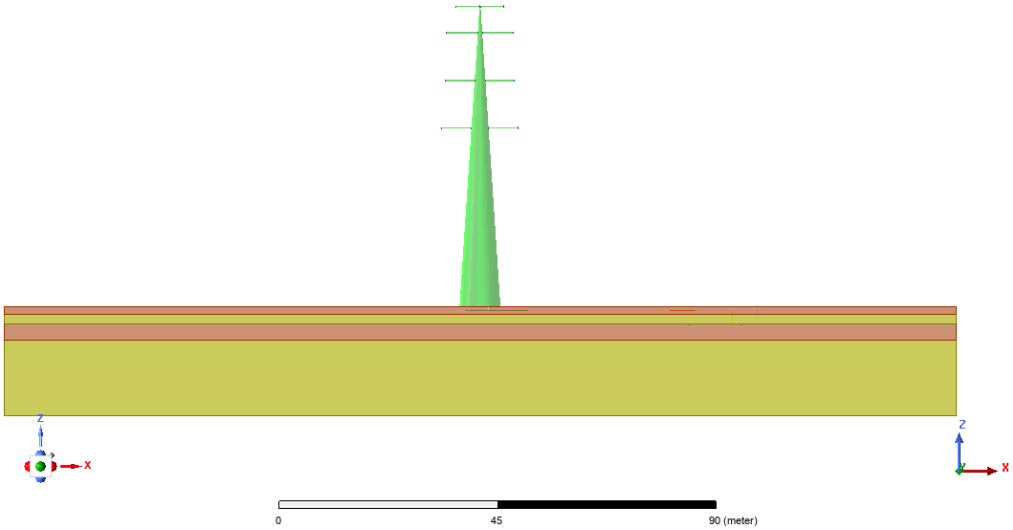


Figure 6. 3D model of the pole with the grounding installation.

The grounding-system geometry implemented in the FEM was based on the technical documentation of the selected tower. A galvanized steel strip with a cross-section of 25 × 4 mm was used as the horizontal grounding conductor. The grounding system comprised three vertical rods with a length of 3 m and four rods with a length of 1.5 m, resulting in a total vertical electrode length of 15 m. The rods had a diameter of 17.2 mm and were located approximately 4 m from the center of the tower footing. The upper part of the vertical electrodes was located at a depth of approximately 0.9 m below the ground surface. The arrangement of the grounding electrodes in the numerical model reproduced the configuration specified in the technical documentation.

The vertical electrodes were arranged diagonally in the vicinity of two tower legs, reproducing the grounding configuration adopted for the selected structure.

The soil domain was represented by three geotechnical layers: layer A from 0 to 1.6 m, layer B from 1.6 to 3.6 m, and layer C from 3.6 to 7.0 m. The corresponding low-frequency soil resistivities were 40, 200, and 40 Ωm. To account approximately for the frequency dependence of the soil electrical properties in the transient calculation, effective material parameters were evaluated at a representative frequency of 25 kHz using a literature-based frequency-dependent soil model. The resulting bulk conductivities were 0.025410 S/m for layers A and C and 0.005265 S/m for layer B. The corresponding relative permittivities were 346.3 for layers A and C and 228.5 for layer B. Relative permeability was set to 1 for all soil

layers. The 25 kHz value is used only to determine effective material parameters; it does not represent a single frequency of the broadband 10/350 µs excitation.

The use of a representative frequency of 25 kHz serves as an approximation of the frequency-dependent electrical properties of the soil under broadband lightning excitation; this can lead to discrepancies between the calculated and actual response of a grounding system, particularly during the initial phase of the impulse, which is characterized by a high rate of current rise.

Accordingly, the adopted soil representation should be regarded as an effective-frequency approximation rather than a fully dispersive soil model. Nonlinear soil ionization was not included in the present analysis.

To account approximately for the frequency dependence of the soil electrical properties, the effective conductivity and relative permittivity of the individual soil layers were determined using the Alípio–Visacro (AV) model. The model was developed on the basis of field measurements of different soils and provides frequency-dependent expressions for soil conductivity and relative permittivity in the frequency range from 100 Hz to 4 MHz [26]. The frequency-dependent conductivity is expressed as

$$\sigma_g(f) = \sigma_0 + \sigma_0 h(\sigma_0)\left(\frac{f}{1\times 10^6}\right)^{\xi} \tag{1}$$

where σ_0 is the low-frequency soil conductivity and

$$h(\sigma_0) = 1.26\sigma_0^{-0.73}. \tag{2}$$

The corresponding relative permittivity is calculated as

$$\varepsilon_r(f) = \frac{\varepsilon'_\infty}{\varepsilon_0} + \frac{\tan(\pi\xi/2)\times 10^{-3}}{2\pi\varepsilon_0(1\times 10^6)^{\xi}}\sigma_0 h(\sigma_0) f^{\xi-1}, \tag{3}$$

where $\xi = 0.54$, $\varepsilon'_\infty/\varepsilon_0 = 12$, and ε_0 is the vacuum permittivity. In the above expressions, σ_0 used in the empirical AV parameterization is expressed in mS/m.

For the present FEM analysis, the effective soil parameters were evaluated at a representative frequency of $f_{\text{eff}} = 25$ kHz. This frequency is not interpreted as the frequency of the 10/350 µs lightning-current waveform, which is inherently broadband. It is used only to determine a single set of effective electrical parameters for each soil layer for implementation in the time-domain FEM. Therefore, the adopted approach represents an effective-frequency approximation of the frequency-dependent soil behavior rather than a fully dispersive material model.

The geotechnical model consisted of three soil layers. Layers A (0–1.6 m) and C (3.6–7.0 m) had a low-frequency resistivity of 40 Ωm, corresponding to $\sigma_0 = 0.025$ S/m, whereas layer B (1.6–3.6 m) had a resistivity of 200 Ωm, corresponding to $\sigma_0 = 0.005$ S/m. Application of the AV model at 25 kHz resulted in the effective parameters listed in Table 1.

Table 1. Electrical parameters of the soil layers used in the transient FEM.

Layer	Depth [m]	ρ_0 [Ωm]	σ_{eff} [S/m]	$\varepsilon_{r,\text{eff}}$
A	0–1.6	40	0.025410	346.3
B	1.6–3.6	200	0.005265	228.5
C	3.6–7.0	40	0.025410	346.3

These effective values were assigned as fixed material properties in ANSYS Maxwell. Consequently, the numerical model accounts approximately for the influence of frequency on soil conductivity and permittivity, but it does not reproduce their continuous variation over the complete frequency spectrum of the lightning-current waveform.

The transient simulation was performed for the selected tower grounding system using a 10/350 µs lightning-current waveform (Figure 7). The waveform was selected to represent a direct-lightning-current excitation scenario.

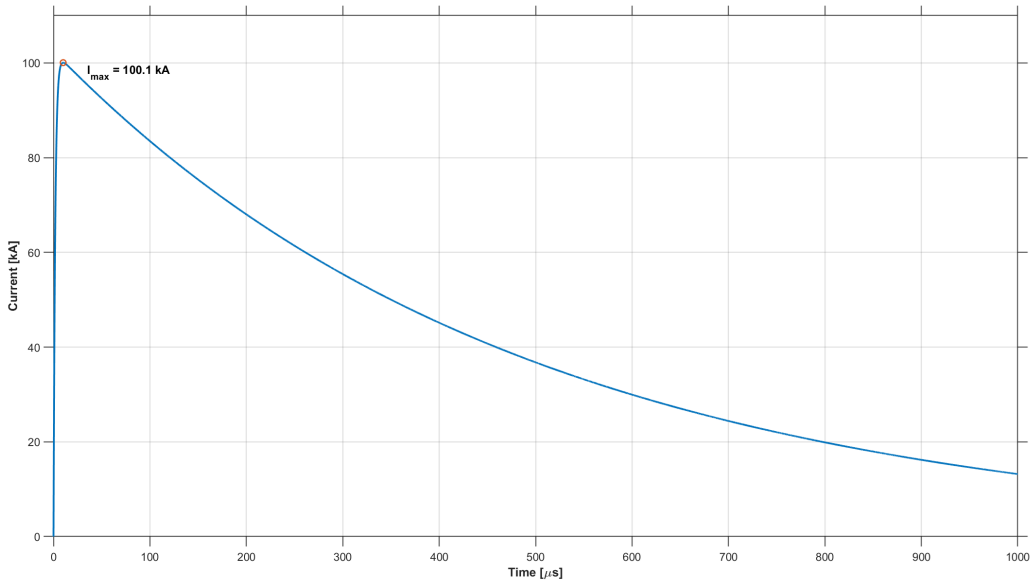


Figure 7. Adopted 10/350 µs lightning-current waveform used in the transient FEM analysis.

The impulse was described by the equation:

$$i(t) = I_0 \cdot k \cdot \left(e^{-a \cdot t} - e^{-b \cdot t}\right) \tag{4}$$

where $I_0 = 100$ kA, $k = 1.025$, $a = 2.05 \times 10^3$ s^{-1}, and $b = 5.64 \times 10^5$ s^{-1} [27]. The adopted double-exponential fitting constants correspond to a published approximation of the 10/350 µs lightning-current waveform [28]. For the selected amplitude, the resulting peak current is approximately 100 kA.

In the FEM, the total transient-current excitation was distributed equally among four current terminals assigned to the tower structure. The current applied to each terminal was therefore defined as

$$i_j(t) = 25 \text{ kA} \cdot 1.025\left(e^{-2.05 \times 10^3 t} - e^{-5.64 \times 10^5 t}\right), \qquad j = 1, \ldots, 4. \tag{5}$$

The sum of the four imposed current excitations produces the approximately 100 kA peak waveform defined above. The four current excitations were directed into the corresponding tower terminals.

A zero-potential boundary condition ($V = 0$ V) was assigned to the selected external boundary of the computational soil domain and was used as the reference potential for the transient electric-field solution.

The computational domain was discretized using the three-dimensional Classic meshing method available in ANSYS Maxwell. The same geometrical model and meshing approach were retained for the final transient calculation. Because the grounding conductors include millimeter-scale cross-sections while the surrounding soil domain extends over meter-scale distances, the model contains a large geometrical scale ratio; this was taken into account when selecting a numerically stable mesh configuration (Figures 8–11).

The transient solution was calculated from 0 to 1.3 ms. The initial time step was 0.05 µs, the maximum time step was 1 µs, and the temporal tolerance was 0.005. The initial electric potential was set to 0 V. Field solutions required for post-processing were stored for the final calculation.

The main parameters of the final transient FEM are summarized in Table 2.

Table 2. Main parameters of the transient FEM.

Parameter	Value/Assumption
Software/solver	ANSYS v. 2026 R1/Maxwell 3D Electric Transient
Analysis domain	Time domain
Current waveform	10/350 µs, double exponential
Total peak current	approximately 100 kA
Current injection	four equal current terminals
Simulation interval	0–1.3 ms
Initial/maximum time step	0.05 µs/1 µs
Temporal tolerance	0.005
Mesh method	Classic 3D mesh
Soil layers	A: 0–1.6 m; B: 1.6–3.6 m; C: 3.6–7.0 m
σ_{eff} (A/B/C)	0.025410/0.005265/0.025410 S/m
$\varepsilon_{r,\text{eff}}$ (A/B/C)	346.3/228.5/346.3
Representative frequency	25 kHz (material-parameter evaluation only)
Soil ionization	Not included

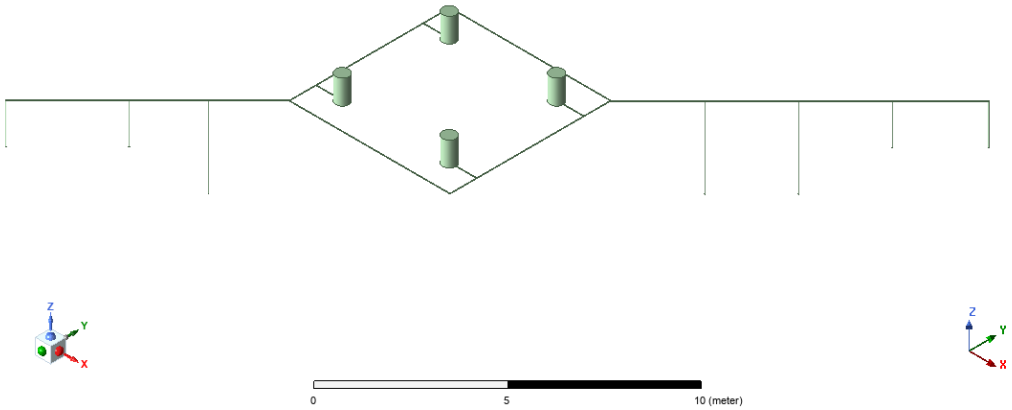


Figure 8. 3D model of the pole grounding installation.

3.2. Transient Current-Density and Electric-Potential Distributions

The transient response of the selected grounding system was evaluated in terms of the current-density and electric-potential distributions within the tower grounding system and the surrounding soil.

For the field distribution evaluated at approximately $t = 10$ µs, i.e., in the vicinity of the peak of the applied 10/350 µs lightning-current waveform, the spatial maximum of the current density was approximately 8.33×10^4 A/m^2. The current-density distribution was strongly non-uniform, with the largest local values concentrated in the vicinity of the tower-footing and grounding-electrode regions, where the injected current is transferred from the metallic structure into the surrounding soil. This value represents the spatial maximum at the reported time instant and should not be interpreted as the global maximum over the entire transient without a separate time-history evaluation.

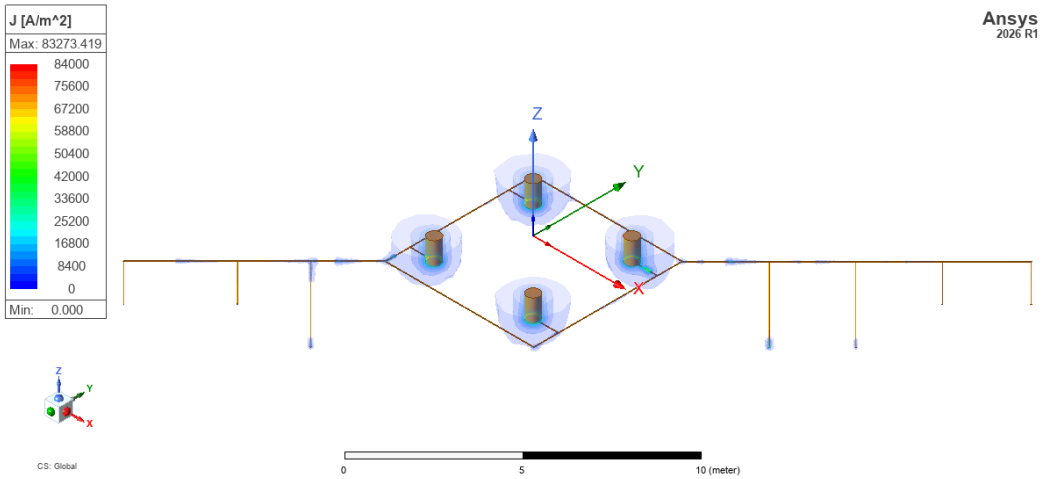


Figure 9. Current density distribution in the pole grounding system.

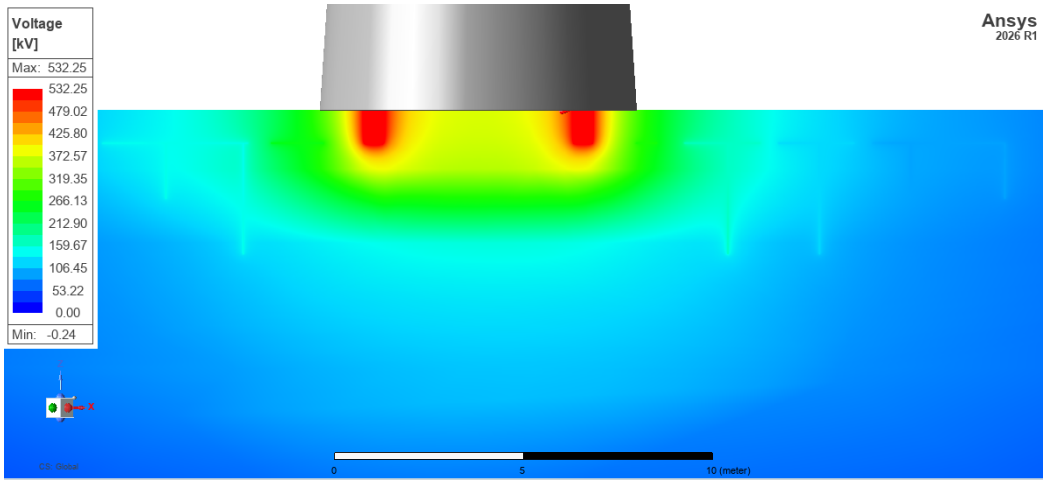


Figure 10. Potential in the pole grounding installation—side view.

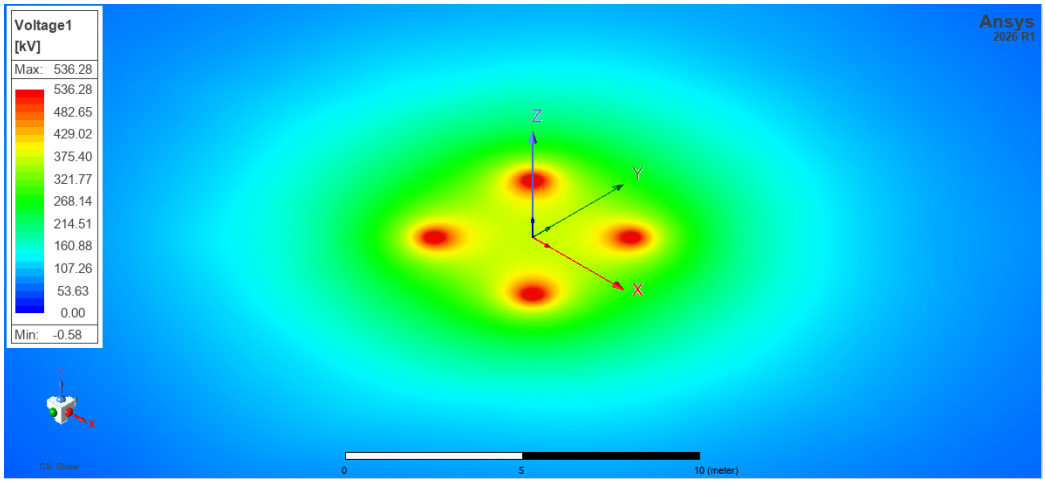


Figure 11. Potential in the pole grounding installation—top view.

For the electric-potential distribution evaluated at approximately $t = 10$ µs, i.e., in the vicinity of the peak of the applied current waveform, the maximum displayed potential was approximately 536.3 kV in the top-view field plot and approximately 532.3 kV in the presented cross-section. The highest local potential values occurred in the immediate vicinity of the tower-footing regions, forming four pronounced high-potential zones associated

with the current-injection regions. The potential decreased progressively with increasing distance from the grounding system. The reported values correspond to the displayed field distributions at the selected time instant and are not presented as global maxima over the complete transient.

The presented distributions of electric potential and current density for $t = 10\,\mu s$ characterize the system's response near the peak of the pulse; conversely, during the decay phase—for instance, at $t = 50\,\mu s$ and $t = 100\,\mu s$—one should expect further temporal evolution, reflecting the reduction in the current excitation and a change in the current distribution within the ground.

The calculated current-density and electric-potential distributions are strongly non-uniform in the vicinity of the individual tower-footing regions. Local differences in the field distribution are consistent with the asymmetrical arrangement of the vertical grounding electrodes represented in the numerical model, while the multilayer electrical structure of the surrounding soil may additionally influence the resulting current paths.

The transient FEM analysis provides information on the spatial distribution of electric potential and current density for the adopted grounding geometry, multilayer soil representation, and prescribed current excitation. The field measurements independently demonstrate that the investigated grounding system satisfies the adopted low-frequency grounding-resistance criterion. However, the measured grounding resistance should not be interpreted as direct experimental validation of the transient response of the grounding system.

Therefore, the transient results presented in this study are used to analyze the predicted redistribution of current and electric potential within the adopted numerical model rather than to confirm the complete lightning impulse performance of the grounding system.

4. Discussion

Power grids, devices and their components are at risk from atmospheric overvoltages [29,30]. As part of the grounding assessment, a specially designed suspension tower and an M1 tension tower were considered as detailed case studies. A special foundation was constructed for the suspension tower. A 25 × 4 mm tape was used to ground the pole, along with three 3 m rods and four 1.5 m rods. The 17.2 mm diameter rods were placed four meters from the center of the footing at a depth of 0.9 m. The total length of the vertical grounding electrodes was 15 m. This is due to the difficult ground conditions. Geotechnical studies indicate that the ground is peat/mud. The soil condition can be assessed as non-bearing, plastic, and moderately compacted, with groundwater at a high level of 0 m. Therefore, the ground resistance calculations assumed a very wet soil moisture condition. This requires taking into account the seasonal soil resistivity coefficient of level 2. For the selected suspension-tower case, the measured resistance is approximately 2.67 Ω. After taking into account ground conditions, the calculated grounding resistance of the pole is 5.34 Ω. This value is significantly below the standard value of 15 Ω [25].

For the tension tower, an M1 tower with a 15-m elevation was considered. The pole was placed on a monolithic foundation. To ground the pole, a similar size of tape was used as for the suspension tower, two 3-m-long rods were used, and four 1.5-m-long rods were used. The arrangement of the grounding rods relative to the tension-tower foundation was similar to the grounding of the suspension tower. The total length of the vertical grounding electrodes was 12 m, which is slightly shorter than the length of the rods manufactured for the special suspension tower. The ground conditions of the pole in question are more favorable for constructing a grounding system that meets the standard resistance values. Geotechnical studies conducted to a depth of seven meters indicate that the soil is cohesive, primarily clay, mixed with sand below 2.4 m. The soil condition can be assessed as plastic and semi-solid, with groundwater at a level of 0.7 m. Therefore, the ground moisture content was assumed to be damp in the grounding-resistance calculations. This requires

taking into account the lower coefficient of seasonal changes in soil resistivity compared to the special suspension tower, which is 1.2. For the selected tension-tower case, the measured resistance is approximately 6.12 Ω. After taking into account the ground conditions, the calculated grounding-resistance value for the pole is 7.34 Ω. This value is higher than the value obtained for the special suspension tower grounding system, but is below the standard value.

Furthermore, it should be noted that due to the very difficult and varied ground conditions of individual poles, the large number of poles and the general provisions of the technical documentation, the selection of the number of grounding rods was made as part of the construction and assembly works.

The comparison of the two selected tower locations demonstrates that the total length of the vertical grounding electrodes alone is not sufficient to characterize grounding performance. The first analyzed tower, equipped with 15 m of vertical electrodes, exhibited a measured grounding resistance of approximately 2.67 Ω, whereas the second tower, equipped with 12 m of vertical electrodes, exhibited a measured value of approximately 6.12 Ω. The difference indicates the combined influence of electrode configuration and local geotechnical conditions on the measured grounding resistance.

The numerical results complement the field measurements by illustrating the non-uniform current-density and electric-potential distributions predicted for the selected grounding configuration. The results indicate that the transient current distribution within the numerical model is spatially non-uniform, emphasizing the importance of representing the actual electrode arrangement and soil stratification in FEM analyses of transmission-tower grounding systems.

An important limitation of the present study is that the field measurements and transient simulations represent different electrical conditions. The three-electrode method provides a low-frequency grounding-resistance value, whereas the numerical model considers the response to a prescribed transient current waveform. Consequently, the field measurements cannot be regarded as direct validation of the transient grounding impedance.

The transient model uses frequency-adjusted effective soil parameters evaluated at a representative frequency of 25 kHz. This treatment accounts approximately for the variation in soil conductivity and permittivity with frequency but does not constitute a fully dispersive material model over the complete spectrum of the 10/350 μs waveform. Nonlinear soil ionization was also not included. Both effects may influence the response during high-amplitude current injection and should be addressed in future experimental and numerical investigations.

The transient calculations should therefore be interpreted within the assumptions of the adopted electric transient FEM formulation and the assigned material properties. The present model does not represent the complete electromagnetic response of the tower–grounding system, including all inductive and wave-propagation effects associated with a lightning event. Consequently, the calculated transient field distributions should be interpreted as results obtained under the adopted modeling assumptions rather than as a complete prediction of the lightning impulse performance of the tower grounding system.

5. Conclusions

This article comprehensively considers the method of installing grounding and ensuring the standard grounding resistance level in 400 kV overhead lines. Therefore, this article presents:

- An analysis of the grounding installation of two selected 400 kV overhead line poles, taking into account ground conditions based on geotechnical documentation. For this purpose, boreholes were drilled to a depth of 7 m and grounding resistance

measurements were performed based on technical documentation and terrain conditions. Detailed assumptions and requirements for the grounding installation for selected 400 kV overhead line poles were presented to achieve the standard grounding resistance values.

- A three-dimensional transient FEM of a selected 400 kV overhead-line tower grounding system was solved in ANSYS Electronics Desktop 2026 R1 using the Maxwell 3D Electric Transient solver. The model incorporated the actual grounding-electrode arrangement and the multilayer soil structure derived from geotechnical documentation. A 10/350 µs double-exponential current waveform with an approximately 100 kA peak value was applied, and frequency-adjusted effective soil parameters evaluated at 25 kHz were used in the transient calculation.
- The field grounding-resistance measurements and the transient FEM analysis should be regarded as complementary rather than directly equivalent assessments. The field measurements characterize the low-frequency grounding resistance, whereas the numerical analysis provides information on the transient field distribution predicted by the adopted FEM. Direct experimental validation of the transient grounding response would require dedicated impulse-current measurements.
- For the transient field distributions evaluated at approximately $t = 10$ µs, corresponding to the vicinity of the peak of the applied 10/350 µs current waveform, the spatial maximum of current density was approximately 8.33×10^4 A/m^2. The maximum displayed electric potential was approximately 536.3 kV in the top-view field plot and approximately 532.3 kV in the presented cross-section. Both quantities exhibited strongly non-uniform spatial distributions in the vicinity of the tower footings and grounding electrodes. These values refer to the reported time instant and are not presented as global maxima over the complete transient.
- A comprehensive analysis of grounding-resistance levels was performed for 16 actual 400 kV overhead-line tower locations, including eight towers located within one relatively uniform area and eight towers located in geotechnically diverse areas. The results show that the measured grounding resistance is influenced by both the electrode arrangement and local soil and moisture conditions. The field data therefore provide site-specific information on low-frequency grounding performance, while the transient FEM provides complementary information on the predicted field distribution under the adopted lightning-current excitation.

Author Contributions: Conceptualization, M.B.; writing—original draft preparation, M.B.; writing—review and editing, M.B. visualization, M.B., P.K. and M.C. All authors have read and agreed to the published version of the manuscript.

Funding: Ministry of Science and Higher Education. No Grant Number (The publication is funded by the Ministry of Science and Higher Education under the 423 'Vectors of Science' programme.)

Data Availability Statement: The data presented in this study are available on request from the corresponding author. (please specify the reason for restriction, e.g., the data are not publicly available due to privacy or ethical restrictions.)

Conflicts of Interest: The authors declare no conflicts of interest.

References

1. Borecki, M. Influence of Spark Gap Parameters on the Strength of the Surge Protection Device and the Method of Its Selection. *Energies* **2023**, *16*, 4974. [CrossRef]
2. Borecki, M.; Ciuba, M.; Kharchenko, Y.; Khanas, Y. Main aspects influencing the evaluation of atmospheric overvoltages in high-voltage networks. *Bull. Pol. Acad. Sci. Tech. Sci.* **2021**, *69*, e135838. [CrossRef]

3. Usman, M.; Park, K.-H.; Lee, B.-W. Analysis of Lightning Transient Characteristics of Short-Length Mixed MMC-MVDC Transmission System. *IEEE Access* **2023**, *11*, 72990–73006. [CrossRef]
4. Cao, J.; Du, Y.; Ding, Y.; Li, B.; Qi, R.; Zhang, Y.; Li, Z. Lightning Surge Analysis of Transmission Line Towers with a Hybrid FDTD-PEEC Method. *IEEE Trans. Power Deliv.* **2022**, *37*, 1275–1284. [CrossRef]
5. Rosales-Asensio, E.; Colmenar-Santos, A.; Rosales, J.C. *Transmission Line Design Manual*; Nova Science Publishers: New York, NY, USA, 2020; Volume 2, pp. 115–140. Art. No. TL-2020-07. [CrossRef]
6. Wang, C.; Liang, X.; Adajar, E.P.; Loewen, P. Investigation of Seasonal Variations of Tower Footing Impedance in Transmission Line Grounding Systems. *IEEE Trans. Ind. Appl.* **2021**, *57*, 4051–4060. [CrossRef]
7. Salarieh, B.; De Silva, J.; Kordi, B. High frequency response of grounding electrodes: Effect of soil dielectric constant. *IET Gener. Transm. Distrib.* **2020**, *14*, 2915–2921. [CrossRef]
8. Visacro, S.; Vale, M.H.M.; Pereira, B.; Silveira, F.H. Differences in the response of transmission lines subjected to the currents of negative and positive lightning flashes: Influence of ground terminations. *Electr. Power Syst. Res.* **2023**, *223*, 109568. [CrossRef]
9. Fitriani, A.; Panjaitan, J.; Syahputra, S.A. The Effect of Soil Type on Touch Voltage and Step Voltage in the Grid Grounding System. *ELKHA J. Tek. Elektro* **2024**, *16*, 56–62. [CrossRef]
10. Nazari, M.; Moini, R.; Fortin, S.; Dawalibi, F.P.; Rachidi, F. Impact of Frequency-Dependent Soil Models on Grounding System Performance for Direct and Indirect Lightning Strikes. *IEEE Trans. Electromagn. Compat.* **2021**, *63*, 134–144. [CrossRef]
11. Gouda, O.E.; El Dein, A.Z.; Yassin, S.; Lehtonen, M.; Darwish, M.M.F. Investigation of soil resistivity impacts on the electrodes of grounding system subjected to lightning strikes. *IET Gener. Transm. Distrib.* **2024**, *18*, 3392–3406. [CrossRef]
12. de Araújo, A.R.J.; Colqui, J.S.L.; de Seixas, C.M.; Kurokawa, S.; Salarieh, B.; Filho, J.P.; Kordi, B. Computation of ground potential rise and grounding impedance of simple arrangement of electrodes buried in frequency-dependent stratified soil. *Electr. Power Syst. Res.* **2021**, *198*, 107364. [CrossRef]
13. Raizer, A.; Elias, E.P.; da Silva, J.V.; Ferreira da Luz, M.V.; Coelho, V.L.; Raupp, V.M.A.; Telló, M. A comparative analysis of grounding in different structures: Operational vs. finite element method models. *Electr. Power Syst. Res.* **2024**, *230*, 110243. [CrossRef]
14. Sun, Q.; Huang, L.; Zhong, X.; Yang, J.; Zhong, L.; Chen, S.; Jin, H. Influence of photovoltaic support on lightning transient under direct lightning strike. *Electr. Power Syst. Res.* **2023**, *214*, 108841. [CrossRef]
15. Borecki, M.; Ciuba, M. Testing of Selected Surge Protection Devices in the Context of the Possibility of Ensuring the Reliability of Power Grids. *Energies* **2023**, *16*, 1445. [CrossRef]
16. Borecki, M.; Kharchenko, Y. Comparative Simulation Analysis of Selected Medium and High Voltage Surge Protection Devices. *Energies* **2022**, *15*, 4326. [CrossRef]
17. Guo, Z.; Wu, G.; Chen, S.; Zhang, Y.; Wei, W. Transient Behavior of Common Grounding Grids to Artificially Triggered Lightning. *IEEE Trans. Electromagn. Compat.* **2019**, *61*, 426–433. [CrossRef]
18. Xue, J.; Huang, H.; Cai, L.; Xu, Z. Lightning Impulse Impedance and Surface Potential Distribution of 10 kV Distribution Line Tower: Field Test and Simulation. *IEEE Trans. Power Deliv.* **2021**, *36*, 415–422. [CrossRef]
19. Sengar, K.P.; Chandrasekaran, K. Transient Analysis of Earthing Electrodes Considering Soil Ionization Phenomenon under Lightning Impulse Condition. *Electr. Eng.* **2024**, *106*, 3083–3096. [CrossRef]
20. Silveira, F.H.; Visacro, S. Lightning Performance of Transmission Lines: Impact of Current Waveform and Front-Time on Backflashover Occurrence. *IEEE Trans. Power Deliv.* **2019**, *34*, 2145–2151. [CrossRef]
21. Raizer, A.; Elias, E.P.; Ferreira da Luz, M.V.; Coelho, V.L.; Raupp, V.M.A.; Telló, M.; Júnior, J.M.G. Traditional and alternative grounding system's impedance and resistance measurements of a 138 kV transmission line tower. *Electr. Power Syst. Res.* **2024**, *231*, 110358. [CrossRef]
22. Liu, S.; Sima, W.; Yuan, T.; Luo, D.; Bai, Y.; Yang, M. Study on X-ray imaging of soil discharge and calculation method of the ionization parameters. *IEEE Trans. Power Deliv.* **2017**, *32*, 2013–2021. [CrossRef]
23. Gouda, O.E.; El Dein, A.Z.; Al-Harthi, M.M.; Omar, S.Y.; Ghoneim, S.S.M. Performance of Grounding Electrodes Under Lightning Strokes in Uniform and Two-Layer Soils Considering Soil Ionization. *IEEE Access* **2022**, *10*, 76855–76869. [CrossRef]
24. Wołkowiński, K. *Uziemienia Urządzeń Elektroenergetycznych [Grounding of Power Engineering Devices]*, 4th ed.; Wydawnictwa Naukowo-Techniczne: Warsaw, Poland, 1972; pp. 85–120.
25. Polskie Sieci Elektroenergetyczne S.A. *PSE Technical Standards: Guidelines for Design and Construction of Overhead Power Line Grounding (Doc. No. PSE-TS.UZIEM.LN.PL2025v1)*; PSE: Konstancin-Jeziorna, Poland, 2025; pp. 1–13.
26. Alípio, R.; Visacro, S. Modeling the Frequency Dependence of Electrical Parameters of Soil. *IEEE Trans. Electromagn. Compat.* **2014**, *56*, 1163–1171. [CrossRef]
27. Wang, J.; Zhang, X. Double-exponential expression of lightning current waveforms. In Proceedings of the 2006 4th Asia-Pacific Conference on Environmental Electromagnetics (CEEM'2006), Dalian, China, 1–4 August 2006; pp. 320–323.
28. Tao, S.; Zhang, X.; Wang, Y.; Yang, J. Transient Behavior Analysis of Offshore Wind Turbines During Lightning Strike to Multi-Blade. *IEEE Access* **2018**, *6*, 22070–22083. [CrossRef]

29. Borecki, M.; Sroka, J. Evaluation of the Effectiveness of Ferrite Characteristics Measurements Based on the CISPR 17 Standard. *IEEE Trans. Magn.* **2022**, *58*, 1–8. [CrossRef]
30. Borecki, M.; Starzyński, J. Selected Aspects of Numerical Models and Cost Comparison Analysis of Surge Protection Device. In Proceedings of the 2018 Progress in Applied Electrical Engineering (PAEE), Koscielisko, Poland, 18–22 June 2018; pp. 1–4. [CrossRef]

Disclaimer/Publisher's Note: The statements, opinions and data contained in all publications are solely those of the individual author(s) and contributor(s) and not of MDPI and/or the editor(s). MDPI and/or the editor(s) disclaim responsibility for any injury to people or property resulting from any ideas, methods, instructions or products referred to in the content.